Batteries & Supercaps

Research Article
doi.org/10.1002/batt.202500450

Chemistry Europe
European Chemical Societies Publishing

www.batteries-supercaps.org

Experimental Study of Capacity Fade in Large Vanadium Redox Flow Battery Cells

Shiv Shankar Kumar and Sreenivas Jayanti*

One of the not so well understood aspects of vanadium redox flow battery cells is the capacity fade that happens during continuous charge–discharge cycles. While several modeling and experimental studies have been reported, reliable data are not available in the open literature. In the present work, long-duration charge–discharge cycling studies are reported in cells of industrial size having an electrode area of about 400 and 1800 cm^2. The continuous current and cell voltage measurements have been supplemented by periodic measurement of concentration of the electro-active vanadium ions in the positive and the negative electrolytes. The weight of the electrolyte tanks and the open circuit voltage of the cell have also been monitored. The mutual self-consistency of these data has been verified by post-test analyses. Data from over thirteen different cases spanning a range of current densities and electrolyte circulation rates show that the capacity fade is about $(0.15 \pm 0.05)\%$ per cycle. In all cases, an asymptotic capacity fade pattern is established in which the concentration of V(V) increased and V(IV) decreased steadily on the positive side, and that of V(III) decreased steadily but slightly on the negative side.

1. Introduction

Access to electrical energy and power have become fundamental and essential needs for everyone. Currently, fossil fuels produce substantial amounts of electrical energy; these are limited in terms of availability, cause air and water pollution, and are also contributing to global warming. Renewable energy sources (RES), such as solar, and wind are potential sources to mitigate the dependency on conventional sources of energy in the future. Typically, RES have a high degree of variability in terms of power generation capability, and the availability of power from RES does not match the actual energy demand.[1] Therefore, energy storage systems (ESS) are essential alternatives to redress this imbalance and thereby enable higher utilization of RES[2] in the energy mix.

In recent years, all-vanadium redox flow batteries (VRFBs)[3] have emerged as being perhaps the most suitable technology for large-scale ESS applications.[4] In these systems, the electroactive species are V^{2+} and V^{3+} (referred to henceforth as V(II) and V(III), respectively) and VO^{2+} and VO_2^+ (referred to henceforth as V(IV) and V(V), respectively) on the positive and the negative sides of the electrochemical cell. All the vanadium ions are dissolved in a strong acid, typically, 3–5 M H_2SO_4. The positive and the negative sides are separated by an ion-exchange membrane, typically, the proton-conducting Nafion membrane. The two electrolytes are stored in separate tanks and are pumped through the battery stack during charging and discharging. As is common to all-liquid flow batteries, the energy storage capacity depends on the volume (and concentration) of the electrolyte, and the power output (or input in case of charging) depends on the size of the cell or stack. The power rating and energy rating of an ESS can be scaled independently.[5]

A VRFB cell converts electrical energy into chemical energy during the process of charging as per the following reactions during the charging process:

Positive side reaction (conversion from V(IV) to V(V))

$$VO^{2+} + H_2O \xrightarrow{\text{Charging}} VO_2^+ + 2H^+ + e^- \quad E^{0+} = +1.004\,\text{V vs. SHE} \tag{1}$$

Negative side reaction (conversion from V(III) to V(II))

$$V^{3+} + e^- \xrightarrow{\text{Charging}} V^{2+} \quad E^{0-} = -0.255\,\text{V vs. SHE} \tag{2}$$

Overall reaction

$$VO^{2+} + V^{3+} + H_2O \xrightarrow{\text{Charging}} VO_2^+ + V^{2+} + 2H^+ \quad E^0 = +1.259\,\text{V vs. SHE} \tag{3}$$

where E^0 is the standard electrochemical potential. All the reactions are heterogeneous reactions occurring on the electron-conducting fibers of the electrode. The protons and the reactant and product species of vanadium ions are in dissolved and dissociated state in the electrolyte. Hence, problems of gas evolution and dendritic growth commonly associated with heterogeneous cell reactions are avoided in the VRFB cells.

Although an ESS based on the all-liquid VRFB has several promising advantages, an important hurdle in commercializing it on a large scale is the issue of capacity fade during long-term charging and discharging. The membranes used in VRFB cells are intended to serve the dual function of being separators of the positive and the negative electrolytes and enabling exchange of protons between the two sides. High protonic conductivity is a desirable feature of the membrane as good energy efficiency

S. S. Kumar, S. Jayanti
Department of Chemical Engineering
Indian Institute of Technology Madras
Chennai 600036, India
E-mail: sjayani@iitm.ac.in

can be maintained even at high current density operation. High protonic conductivity is also usually accompanied by relatively high permeability for the vanadium species. Intermixing of the active vanadium ions on the positive side (V(IV) and V(V)) with those on the negative side (V(III) and V(II)) leads to loss of charge storage capacity due to the following "self-discharge" reactions

On the positive side

$$2VO_2^+ + V^{2+} + 2H^+ \rightarrow 3VO^{2+} + H_2O \quad (\text{due to cross-over of V(II) ion}) \tag{4a}$$

$$VO_2^+ + V^{3+} \rightarrow 2VO^{2+} \quad (\text{due to cross-over of V(III) ion}) \tag{4b}$$

$$VO^{2+} + V^{2+} + 2H^+ \rightarrow 2V^{3+} + 2H_2O \quad (\text{due to cross-over of V(II) ion}) \tag{4c}$$

On the negative side

$$V^{3+} + VO_2^+ \rightarrow 2VO^{2+} \quad (\text{due to cross-over of V(V) ion}) \tag{5a}$$

$$V^{2+} + VO^{2+} + 2H^+ \rightarrow 2V^{3+} + 2H_2O \quad (\text{due to cross-over of V(IV) ion}) \tag{5b}$$

$$2V^{2+} + VO_2^+ + 4H^+ \rightarrow 3VO^{2+} + H_2O \quad (\text{due to cross-over of V(V) ion}) \tag{5c}$$

Apart from these, a number of other factors, such as gas (hydrogen or oxygen) evolution, vanadium ion precipitation and water migration, can contribute to electrolyte imbalance and thus to capacity fade. Of these, gas evolution and vanadium ion precipitation can be avoided by careful design and operation of the cell. Water migration is a clearly visible manifestation in the initial stages of charge–discharge cycling of a VRFB cell and was the subject of early investigations.[6,7] Wiedemann et al.[8] conducted ion exchange equilibria studies of vanadium ions with H_3O^+ ions in three cation exchange membranes and found that all four vanadium ions had significant solubility in the membranes giving rise to the possibility of counter-diffusion of these ions during charge/discharge processes. Sun et al.[9] used a dialysis cell to determine vanadium ion diffusivities through Nafion 115 membrane and found the diffusion coefficients of V(II), V(III), V(IV), and V(V) to be (rounded to one decimal place) 5.3, 1.9, 4.1, and 3.5×10^{-6} $cm^2\,min^{-1}$, respectively. They also conducted self-discharge tests in a kilowatt-scale stack having 15 cells of 850 cm^2 active area each during which they monitored vanadium ion concentration as well as electrolyte volume on each side. Under one charge–discharge cyclic condition, they reported a net vanadium ion cross-over of about 30% from the negative side to the positive and roughly equal amount of volume displacement over 300 cycles. Oriero et al.[10] conducted similar cross-over studies in a 6 kW stack with an anion exchange membrane; these charge/ discharge cycles were each of 8 h duration with a rest period of 4 h after each step. They reported an average of 0.5% volume transfer from the negative side to the positive side in the first 8 cycles. They also reported about significant cross-over of vanadium ions over 25 days during which the SoC was maintained between 50% and 60%.

A number of longer-duration (in terms of number of charge–discharge cycles) studies have been reported[11–19] on capacity fade (see **Table 1**) which highlight the importance of other mechanisms such ion migration, osmosis, and reverse osmosis.[10,19] These have been typically in small cells of 25–100 cm^2 in size. The reported capacity fade varies over a wide range and is rather too high for practical applications. For example, in the three most recent studies reported in the literature, Huang et al.[18] reported, based on studies in a 40 cm^2 active area cell, capacity fade of about 40% in 60 cycles of charge–discharge at current density of 120 mA cm^{-2}. Zou et al.[19] reported capacity fade of between 65% and 80% over 200 cycles in their cell of 25 cm^2 active area when operated in the current density range of 80–200 mA cm^{-2}. Similarly, Ma et al.[20] reported a capacity loss of over 70% within 75 cycles and more than 95% over 200 cycles when their 25 cm^2 cell was operated over a current density range of 80–150 mA cm^{-2}.

Such large extent and high rate of capacity fade will be inimical to practical applications of VRFB systems. It is possible that small cell results are influenced by the much higher flow rate that is usually employed. A 100-cycle study conducted[21] in a 426 cm^2

Table 1. Compilation of capacity fade data reported in recent literature.

S.no.	Publication [Reference]	Cell area [cm^2]	Voltage range [V]	Membrane type	Current density [mA cm^{-2}]	Initial capacity [Ah]	Final capacity [Ah]	Number of cycles	Total % capacity fade	% capacity fade per cycle
1	Huang et al. 2024[18]	40	1.65–1.10	Nafion 117	120	–	–	60	38.24	0.637
2	Huang et al. 2024[18]	40	1.75–1.10	Nafion 117	120	–	–	60	39.98	0.666
3	Zou et al. 2024[19]	40	1.80–1.10	Nafion 117	120	–	–	60	43.4	0.723
4	Chen et al. 2023[17]	25	1.65–1.00	Nafion 212	150	1.05	0.75	200	28.57	0.143
5	Maghsoudy et al. 2022[16]	2.56	1.70–0.80	Nafion 117	80	–	–	20	13.00	0.650
6	Bhattarai et al. 2018[15]	100	1.65–0.90	Nafion 117	80	3.55	3	100	15.49	0.155
7	Bo et al. 2016[13]	25	1.65–0.80	Nafion 117	80	–	–	200	50.00	0.250
8	Bo et al. 2016[13]	25	1.65–0.80	Nafion 117	160	–	–	200	40.00	0.200
9	Nibel et al. 2016[14]	25	1.7–0.80	Nafion 117	120	1.7	1	35	41.18	1.176
10	Li et al. 2014[12]	25	1.65–0.80	Nafion 117	80	–	–	150	66.00	0.440
11	Dai et al. 2014[11]	25	1.65–0.80	Nafion 117	80	–	–	300	83.80	0.279

area cell at a current density of 60 mA cm^{-2} and electrolyte circulation rate of 0.42 ml min^{-1} cm^2 showed a capacity fade of about 0.2% per cycle. The cell had a serpentine flow field and therefore had low pressure drop. Low values of capacity fades of similar range have been reported by Vudisi et al.[22,23] in a catalytically activated VRFB cell of 936 cm^2 area operated for 100 cycles each at current density of 120 and 150 mA cm^{-2}. An even lower capacity fade of 0.1% per cycle over 200 cycles at 120 mA cm^{-2} was reported by the same researchers[23] in the same cell with thermally activated electrodes without catalytic activation. In contrast, the study of Monteiro et al.[24] in a 25 cm^2 area cell employing area specific flow rate between 1.5 and 6 ml min cm^{-2} showed a capacity fade increasing from 0.38% per cycle to 1.5% per cycle over this range. Bo et al.[13] in a 25 cm^2 area cell employing four Nafion membrane variants found that while its round-trip energy efficiency was lower, Nafion 117 had the best capacity retention showing retention of 50% at the end of 200 cycles at a current density of 80 mA cm^{-2} and 60% at a current density of 160 mA cm^{-2}. In none of the above cases, the variation of vanadium ion concentrations was measured.

In the present work, we propose a comprehensive experimental study aimed at obtaining capacity fade data in VRFB cells of practical sizes and operating conditions. To this end, several long-duration experiments have been conducted in cells of 426 and 1800 cm^2 active area with periodic measurement of vanadium ion concentration in the positive and the negative electrolytes. Simultaneously, the change in weight of the tanks was monitored. The open circuit voltage (OCV) of the cell was measured in-between charging and discharging steps. Taken together, these measurements throw new light on the capacity fade phenomenon in VRFB cells. Details of these studies and the results obtained are discussed below.

2. Results and Discussion

Capacity fade data collection experiments have been run for a number of cases reflecting variation of cell size, current density, electrolyte volume, electrolyte flow rate, type of pump used. While several experiments ran to the desired extent of 400 consecutive charge–discharge cycles set to fixed voltage limits of [0.9, 1.7 V], some had to be abandoned mid-way due to power failure, pump failure, tube failure and excessive seepage; the data of cases where there was a significant loss of electrolyte are not included in the present study. The details of the experimental runs included in the present study for discussion are listed in **Table 2**. The set of cases includes data from four cells, at four current densities, electrode architecture of two types (flow past and flow through modes), different values of electrolyte volume to electrode surface area, and different electrolyte circulation rates.

2.1. Data from Medium-Size Cell

With reference to Table 2, the medium size cell data correspond to those obtained in the flow past-mode cell of 426 cm^2 active area (with serpentine flow field grooved on a 15 mm-thick graphite plate bipolar plate and having an electrode thickness of 3 mm after compression) and in the flow through-mode cell of 440 cm^2 active area (which used 0.6 mm-thick expanded graphite sheet bipolar plate and a 10 mm-thick electrode consisting of three layers of 4.6 mm thick carbon felts). Of the total of 9 data sets, four have been obtained using diaphragm pumps while five have been obtained using peristaltic pumps which required two to three stoppages of the cycling to change the headers. In some cases, these interruptions led to an immediate decrease in the discharge capacity which disappeared slowly, i.e., after several subsequent cycles. There was no loss of electrolyte in these scheduled stoppages. In some cases, there was pump or tube failure leading to leakage and loss of electrolyte; data from such experiments is not included in the present work. With diaphragm pumps, there was no interruption in the charge–discharge cycling. In terms of the flow-past versus flow-through mode cell designs, the former had significantly lower pressure drop; however, over the long course of the run (lasting a week or more), some seepage or "sweating" was found to occur from the sides of the bipolar plates. Since the expanded graphite sheet was impermeable to the electrolyte, no seepage occurred in the flow through mode designs. Also, in two of these nine data sets, the effect of electrolyte volume was studied, while the effect of electrolyte circulation rate was studied in three data sets. In all cases, concentration measurements were made at frequent intervals.

Figure 1 shows typical variation of quantities of interest during a 400-cycle charge–discharge cycling (CDC) test on the medium size cell (426 cm^2 cell area) at a current density of 100 mA cm^{-2} and at an electrolyte circulation rate of 330 ml min^{-1} (Case #5 of Table 2). A gradual loss of capacity is evident in Figure 1a as the CDC progresses. The total number of moles of the four vanadium ions of interest, namely, V(IV) and V(V) on the positive side, and V(III) and V(II) on the negative side, measured at frequent intervals is shown at the end of the discharge step of test. One would expect that at the end of discharge, V(II) on the negative side and V(V) ions on the positive side would be very low and the corresponding V(III) and V(IV) ions would be maximum. While this was true at the beginning, one can observe a more complicated behavior during the first hundred cycles. Thereafter, over the next 300 cycles, the variation goes into a set pattern of steadily increasing V(V) on the positive side with a steady decrease of V(IV) on the positive side and a slower decrease in the concentration of V(III) on the negative side while the concentration of V(II) remains very low at the end of discharge. This is a recurring pattern of asymptotic capacity fade that we have observed in the present series of experiments.

Figure 2 shows the measured variation of several monitored parameters during long CDC testing at three different current densities in the medium size cells. The data shown here correspond to Cases #2, 5, and 8 of Table 2 in which constant current CDC testing was done at current densities of 75, 100, and 125 mA cm^{-2}. In all these cases, the electrolyte volume was 426 ml on each side, and the electrolytes were circulated at the rate of 330 ml min^{-1} using diaphragm pumps for Cases #2, #5, and #8. It can be seen from Figure 2a where the discharge

Research Article
doi.org/10.1002/batt.202500450

Chemistry Europe
European Chemical Societies Publishing

Table 2. Details of the experimental results of the VRFB.

Case No	Cell active area [cm^2]	Electrolyte		Types of bipolar plate	Electrolyte flow rate [ml min^{-1}]	Active area per unit electrolyte volume	Current density [mA cm^{-2}]	Type of pump	No. of cycles	Duration of test [h]	Capacity [Ah] at end of		Capacity fade		
		Volume [ml]	Circulation mode								First discharge	Last discharge	%/cycle	Flux [Ah m^{-2} h^{-1}]	%/day
1	426	426	Flow past	Graphite plate	248	1.00	75	Peristaltic	400	163.93	10.83	1.8	0.208	1.293	12.21
2	426	426	Flow past	Graphite plate	330	1.00	75	Diaphragm	400	254.87	12.96	6.72	0.120	0.519	4.53
3	426	426	Flow past	Graphite plate	166	1.00	100	Peristaltic	400	95.32	7.86	0.9	0.221	1.714	22.29
4	426	426	Flow past	Graphite plate	332	1.00	100	Peristaltic	400	149.19	11.49	2.94	0.186	1.345	11.97
5	426	426	Flow past	Graphite plate	330	1.00	100	Diaphragm	400	156.21	12.44	3.27	0.184	1.378	11.32
6	426	852	Flow past	Graphite plate	330	0.50	100	Diaphragm	340	251.10	18.53	9.99	0.136	0.798	4.40
7	426	426	Flow past	Graphite plate	207	1.00	125	Peristaltic	400	81.95	5.33	2.63	0.127	0.773	14.83
8	426	426	Flow past	Graphite plate	330	1.00	125	Diaphragm	400	118.57	7.04	5.77	0.045	0.251	3.65
9	440	670	Flow through	Graphite sheet	530	0.66	150	Peristaltic	400	105.66	7.43	5.71	0.058	0.370	4.95
10	1800	3100	Flow through	Graphite sheet	1250	0.58	75	Peristaltic	400	551.19	117.56	55.78	0.131	0.623	2.29
11	1800	3100	Flow through	Graphite sheet	1250	0.58	100	Peristaltic	162	172.04	104.46	72.09	0.191	1.045	4.32
12	1800	3100	Flow through	Graphite sheet	1250	0.58	125	Peristaltic	194	143.11	86.78	60.24	0.158	1.030	5.13
13	168	315	Flow through	Graphite sheet	430	0.53	125	Peristaltic	400	242.38	10.22	2.65	0.185	1.859	7.31
											Average		0.150	1.000	8.53
											Standard deviation		0.055	0.502	5.48

Research Article
doi.org/10.1002/batt.202500450
Chemistry Europe
European Chemical Societies Publishing

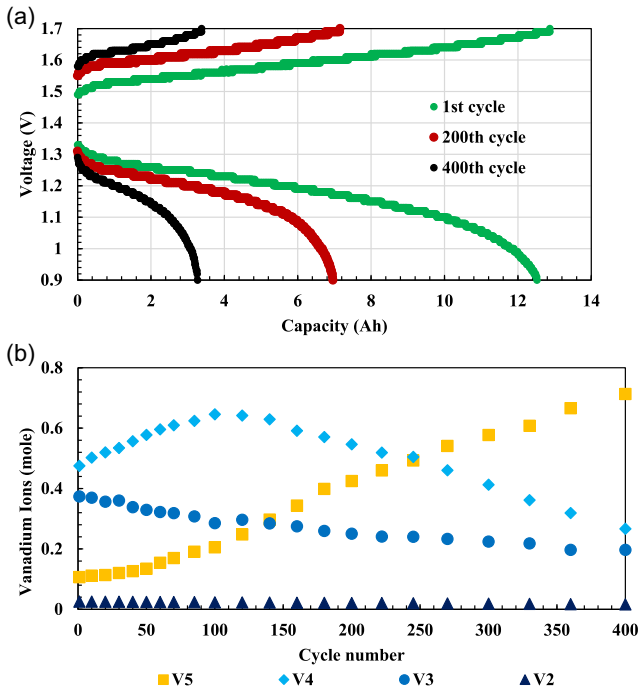

Figure 1. Typical results from the medium size 426 cm^2 VRFB cell (Case# 5) operated at a current density of 100 mA cm^{-2}: top: measured variation of cell voltage with capacity at the end of different cycles as marked. Bottom: variation of vanadium ions (V(IV) and V(V) on the positive side, and V(III) and V(II) on the negative side) at the end of discharge step at the end of different cycles as marked.

capacity is plotted as a function of the cycle number, all three runs retained about 50% of initial capacity by the end of 200 cycles, although the extent of capacity "fade" varied from case to case. Estimation of capacity fade is rendered difficult by the initial discharge capacity, which is affected by the current density. The discharge capacity in the first cycle was substantially lower for cell operation at 125 mA cm^{-2} (Case #8) than for cell operation at 75 mA cm^{-2} (Case #2) or 100 mA cm^{-2} (Case #5). The subsequent capacity variation with progression of CDC testing is significantly different. It may be noted that the duration of the experiments is also substantially different, it being 254 h for Case #2, 156 h for Case #5, and only 118 h for Case #8. The coulombic efficiency (not shown) remained constant and high for all the experiments (over 95%); for Cases #5 and #8, it varied between 96% and 97% over the duration of test while for Case #2, it varied between 95% and 96% over the same duration. Figure 2b shows the variation of the weight of the positive and the negative tanks relative to their initial weight at the beginning of the CDC testing, i.e., after the initial charging was over. Although a linear, and hence steady, rate of mass loss from the negative to the positive side is evident in all the three cases, the lowest rate of change was observed for Case #8 and the highest for Case #5. Figure 2c shows the evolution of the OCV measured in between charge and discharge steps. One can see that with the OCV increases steadily as the test progresses in all cases, the increase being the highest for Case #5 which had the highest capacity fade and the lowest for Case #8 which had the least capacity fade. Figure 2d–f show the variation with cycle number of concentration of vanadium ions (V(IV) and V(V) on the positive side and V(III) and V(II) on the negative side) at the end of the discharge step.

While there are differences in the variation of ion concentrations in the early part of the runs, the asymptotic mode of capacity fade evidenced by steadily increasing concentration of V(V) on the positive side and a corresponding decrease in the concentrations of V(IV) and V(III) is exhibited in all the three cases. Taking

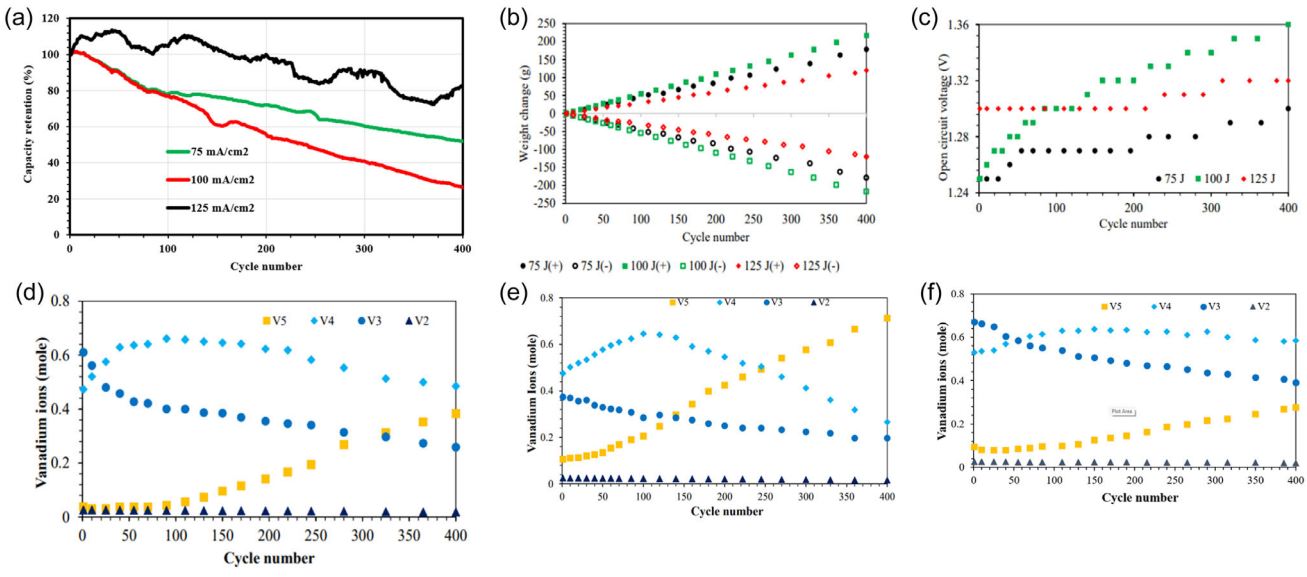

Figure 2. Comparative results of data from 426 cm^2 cell having graphite plates with grooved serpentine channels operated at current density of 75, 100, and 125 mA cm^{-2} for an electrolyte circulation rate of 330 ml/min in all cases (Cases #2, #5, and #8) showing variation with cycle number of a) discharge capacity retention, b) relative weight gain in the electrolyte tank, c) OCV during rest period end of charge, d–f): moles of V(V) and V(IV)in the positive electrolyte and V(III) and V(II) in the negative electrolyte at the end of discharge step.

Research Article
doi.org/10.1002/batt.202500450
Chemistry Europe
European Chemical Societies Publishing

the data of loss of weight in Figure 2b together with the ion concentration data in Figure 2d–f, one can estimate the total moles of vanadium present on each side. These estimates show that as the charge–discharge cycling progressed, there was a gradual net transfer of vanadium ions from the negative side to the positive side.

Figure 3 and **4** show additional data from the medium size cell (426 cm^2) experiments. Figure 3a shows comparative capacity fade data of Cases #5 and #6, both being of identical design and test protocol except that Case #6 had twice the electrolyte volume of that of Case #5. Because of this, the initial discharge capacities were different; however, both showed a fairly linear decrease in capacity with increasing number of cycles. Evidence of vanadium ion concentration changes can be gleaned from the

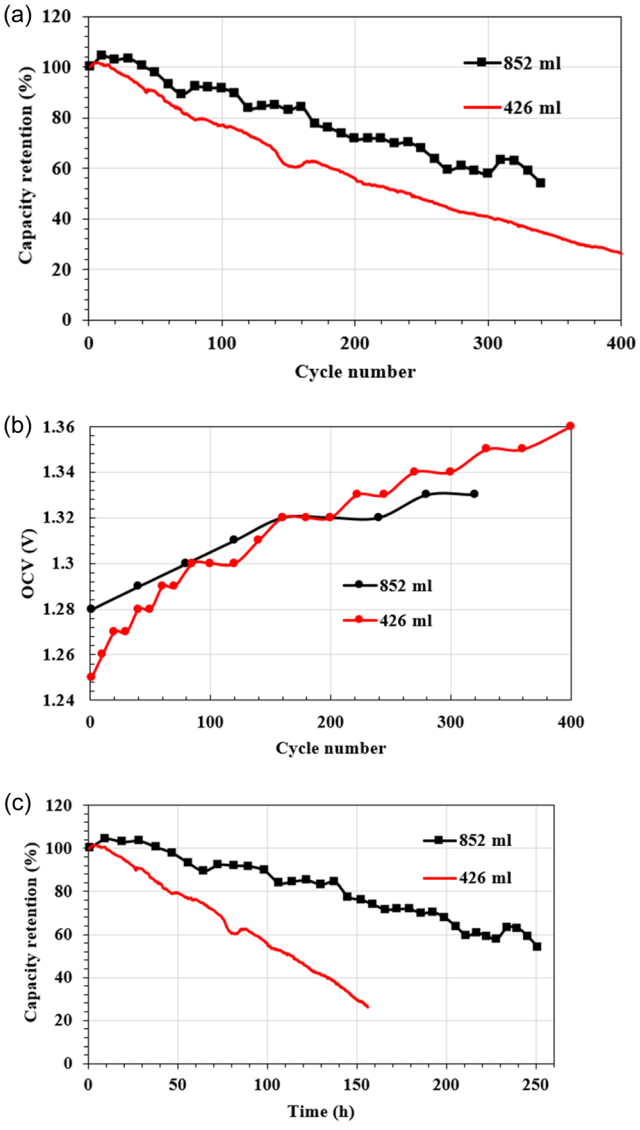

Figure 3. Comparative data from cell of 426 cm^2 having graphite plates with serpentine channels operated at a current density of 100 mA cm^{-2} of a) discharge capacity retention versus cycle number, b) OCV during rest period versus cycle number, and c) capacity fade versus time for electrolyte volume of of 426 ml (Case #5) and 852 ml (Case #6 of Table 2).

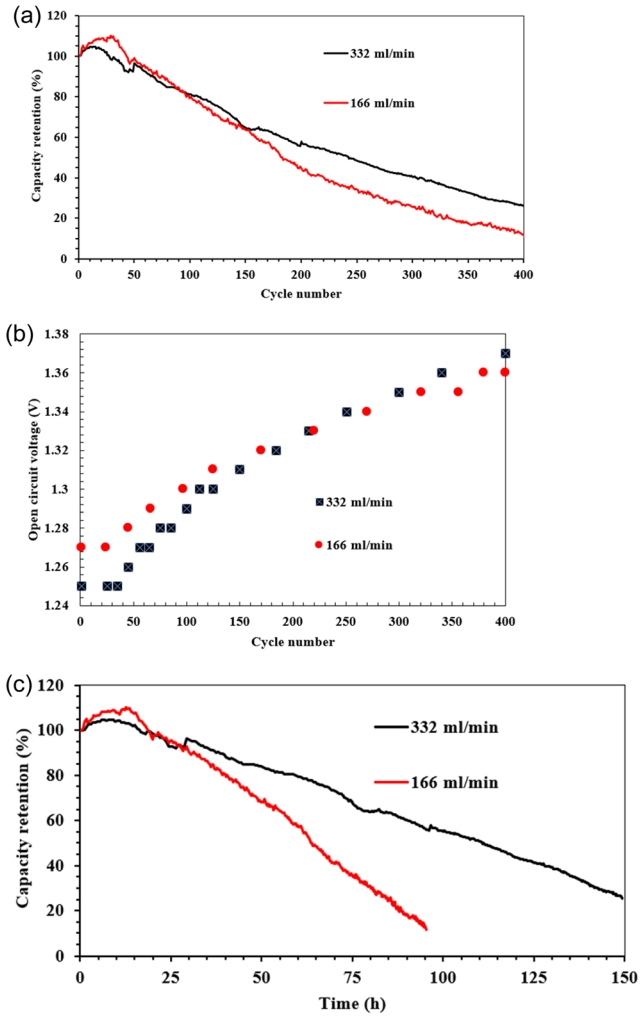

Figure 4. Comparative data from cell of 426 cm^2 having graphite plates with serpentine channels operated at a current density of 100 mA cm^{-2} of a) discharge capacity retention versus cycle number, b) OCV during rest period versus cycle number, and c) capacity fade versus time for circulation rate of 166 ml min^{-1} (Case #3) and 332 ml min^{-1} (Case #4).

gradual increase in the open circuit voltage shown in Figure 3b. One can see here that changes in concentration caused by ion migration and diffusion over the same cell area will have different effects when the electrolyte volumes are different. The same net flux of ions is likely to cause less change in concentration when the electrolyte volume is higher, thus leading to less change in the OCV. This will have further consequences on subsequent migration and diffusional rates. In order to gain further insight into the rate of capacity of fade, the discharge capacity data of Figure 3a is replotted in Figure 3c as a function of time, and a linear fit through each data is also shown. While the slope of the linear variation of capacity with number of cycles is about the same (it is slightly lower for Case #5 with lower electrolyte volume) for the two cases, one can clearly see in Figure 3c that the fade rate on a time basis is clearly higher for Case #5.

The effect of electrolyte circulation rate on capacity fade is studied in a similar way in Figure 4 which compares the discharge capacities (Figure 4a) and open circuit voltage (Figure 4b) for

Research Article
doi.org/10.1002/batt.202500450
Chemistry Europe
European Chemical Societies Publishing

Cases #3 and #4 of Table 2. Both runs were set up identically in all respects except that the electrolyte circulation rate in Case #3 was half of that of Case #4. Both cases completed runs of 400 consecutive charge–discharge cycles. Due to the low circulation rate, Case #3 had lower initial discharge capacity (Figure 4a), presumably due to early onset of mass transfer polarization when the circulation rate and hence the mass transfer rate is low,[21,25] and, on the whole, a higher capacity fade in terms of percentage. The upward drift in the open circuit voltage (Figure 4b) was however less. Replotting the data as a function of time in Figure 4c, one can see that on a time basis, the capacity fade was faster. Similar conclusion of higher capacity fade rate for lower circulation rates can be observed by comparing Cases #1 and #2 of Table 2 showing results for a current density of 75 mA cm^{-2}, and again Cases #7 and #8 showing results obtained for a current density of 125 mA cm^{-2}.

Results shown in Figure 3 and 4 indicate that changing either the volume or the circulation rate can have an effect on the initial state of charge and the number of ions of different oxidation states that are present at the beginning. This will have a subsequent effect on the quantity of diffusion and migration fluxes leading to different evolutions of the capacity over time for different cases. Such effects can be understood quantitatively only by a detailed phenomenological modeling of the underlying causes and effects.

2.2. Experiments in a Large Cell of Flow through Mode Design

Cases #1 to #8 were made in a cell having thick graphite plates as bipolar plates. Over long-duration testing, there would be some electrolyte loss due to sweating and an unknown amount of oxygen as a dissolved gas. The problem would be exacerbated in a large cell due to the higher internal pressure at which the cell would be operating. In view of this, a flow through-mode cell design,[24,26] which had impermeable, thin, expanded graphite sheets as bipolar plates, was used to obtain capacity fade data in large cell of 1800 cm^2 active area. This cell provided a leak-proof environment for long-term testing. The three test runs discussed in this section correspond to Cases #10, #11, and #12 and had 3.1 L of electrolyte on each side. **Figure 5** shows that results obtained for a 400-cycle test that lasted 551 h or close to 23 days of continuous operation. Figure 5a shows the discharge capacity variation with both cycle number and time. One can see a steady decline in discharge capacity as the test progressed, resulting in a total capacity fade of about 53% over 400 cycles. A noticeable feature of this test was that tank weights remained fairly constant after about 20 cycles and showed very little further gain or loss. The open circuit voltage also did not vary much; the increase was limited to only about 20 mV over the first 150 cycles of the test. Figure 5b shows the variation of the vanadium species; the concentration of V(V) showed a steady increase, which was nearly matched by the decrease in the concentration of V(IV) on the positive side and V(III) on the negative side. The measured ion concentrations were used to estimate the state of charge on the

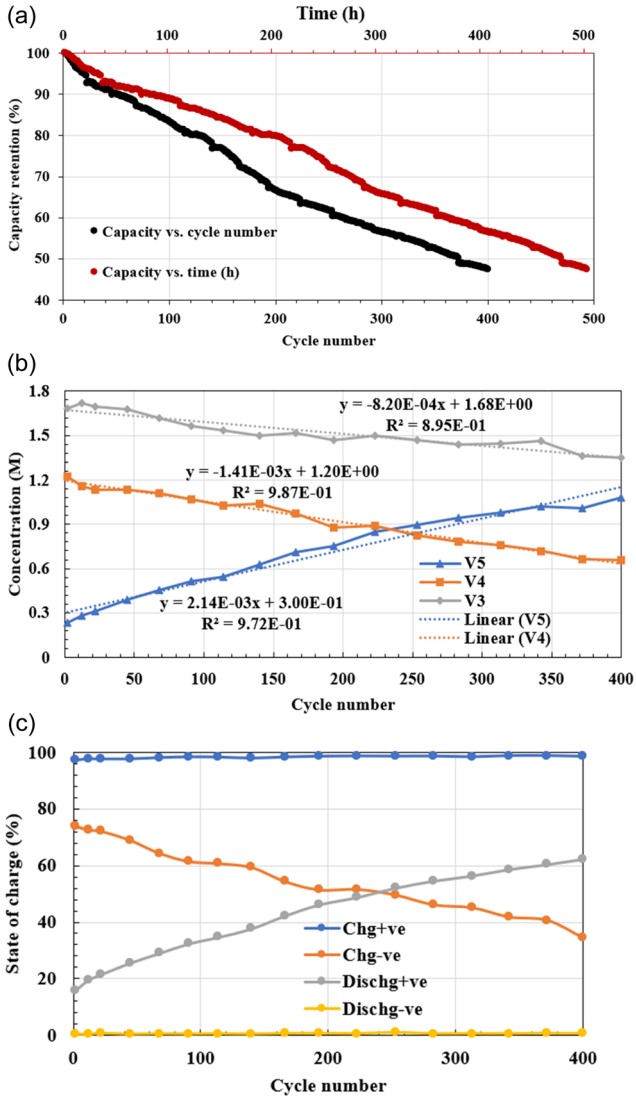

Figure 5. Experimental results for long term study in an 1800 cm^2 cell of flow through mode type operating at 75 mA cm^{-2} with an electrolyte circulation rate of 1250 ml min^{-1} (Case #10): a) variation of discharge capacity retention as a function of cycle number (primary *x*-axis) and time (secondary *x*-axis), b) variation with cycle number of vanadium ion concentrations at the end of discharge step, and c) estimated state of charge on the positive side and negative side at the end of charge and discharge steps.

positive side and the negative side using Equation (8) and (9). These estimated SOCs are plotted as a function of cycle number in Figure 5c. One can see that while the SoC on the negative side remained close to zero throughout, the SOC on the positive side at the end of charge step remained high (over 97%) while on the negative side, it increased from about 16% to 62%, thereby effectively reducing the scope for charge storage. This increase in SOC on the positive side at the end of the discharge step can be attributed to the accumulation and steady increase of V(V) ions, which was also observed in the medium size cell studies.

Figure 6 shows the effect of current density on capacity fade in the large cell. Cases #10, #11, and #12 deal with current densities of 75, 100, and 125 mA cm^{-2} operation of the large cell, respectively. The discharge capacity and vanadium ion

Research Article
doi.org/10.1002/batt.202500450
Chemistry Europe
European Chemical Societies Publishing

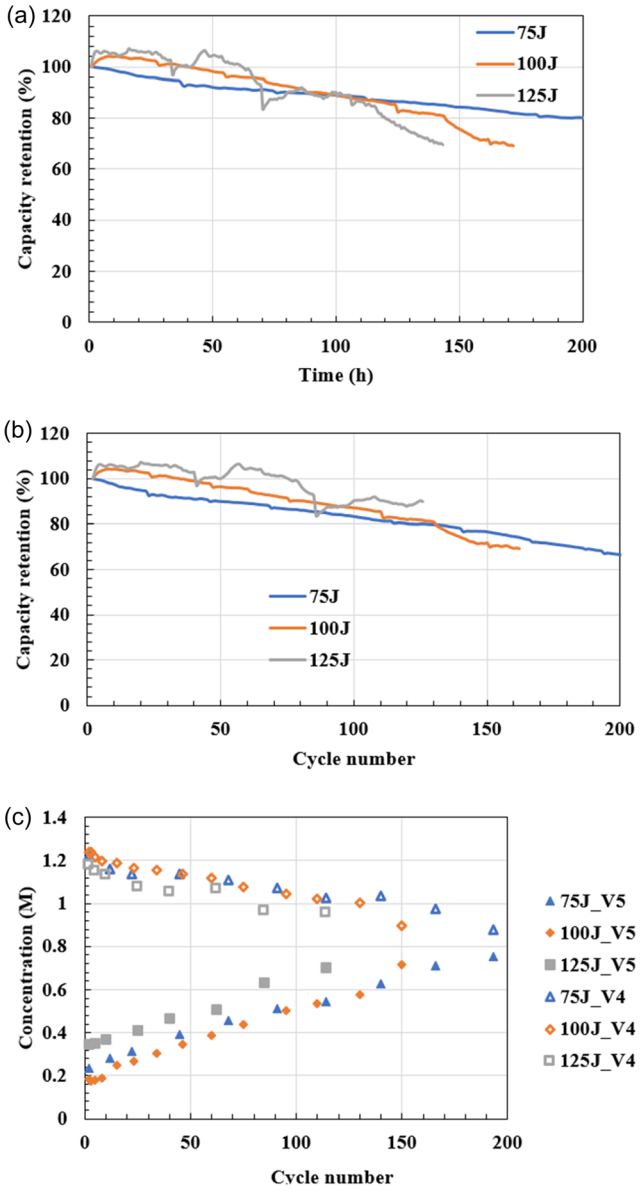

Figure 6. Effect of current density on capacity fade in the large cell (1800 cm^2) of flow through mode type design: experimental results for cases #10, #11, and #12, corresponding to cell operation at current density of 75, 100, and 125 mA cm^{-2}, respectively, at a constant circulation rate of 1250 ml min^{-1}: a) variation of discharge capacity retention with time, b) capacity retention as a function of time, and c) vanadium ion concentrations at the end of discharge step.

concentration measurement data from these runs are shown in this figure. All the three runs had the same electrolyte circulation rate of 1250 ml min^{-1}. As may be expected in such a case, a lower current density operation would yield higher discharge capacity; this is reflected in the data of Figure 6a where the capacity data are compared on an absolute scale. These data are plotted in Figure 6b in terms of capacity retention which is defined as the per centage capacity remaining relative to the discharge capacity of the first cycle. This value goes higher than 100% in the initial stages in the case of Cases #11 and #12, which typically happens for high current density operation. However, the longer-term time-rate of loss of capacity appears to be about the same for the three current densities over the first 150–200 cycles. The pattern of increasing concentration of V(V) and decreasing concentration of V(IV) is repeated in the large cell case too. In this asymptotic capacity pattern, data of concentrations from Cases #11 and #12 too show, as in the case of Figure 5b, that the concentration gain in V(V) is roughly balanced by concentration loss in V(IV) and V(III) put together.

2.3. Comparison of Data from Different Cell Sizes

In order to further see the effect of cell size, experiments have been conducted using a similar protocol on a cell of 168 cm^2 active area with electrolyte volume of 315 ml on each side at the beginning of the experiment. Data corresponding to a current density of 125 mA cm^{-2} (Case #13 of Table 2) are compared in **Figure 7** with those obtained at the same current density in a 426 cm^2 cell (Case #8) and 1800 cm^2 (Case #12) and with data at 150 mA cm^{-2} in a 440 cm^2 cell (Case #9) in terms of normalized discharge capacity of each cycle, which was obtained by dividing the discharge capacity in a cycle by the maximum discharge

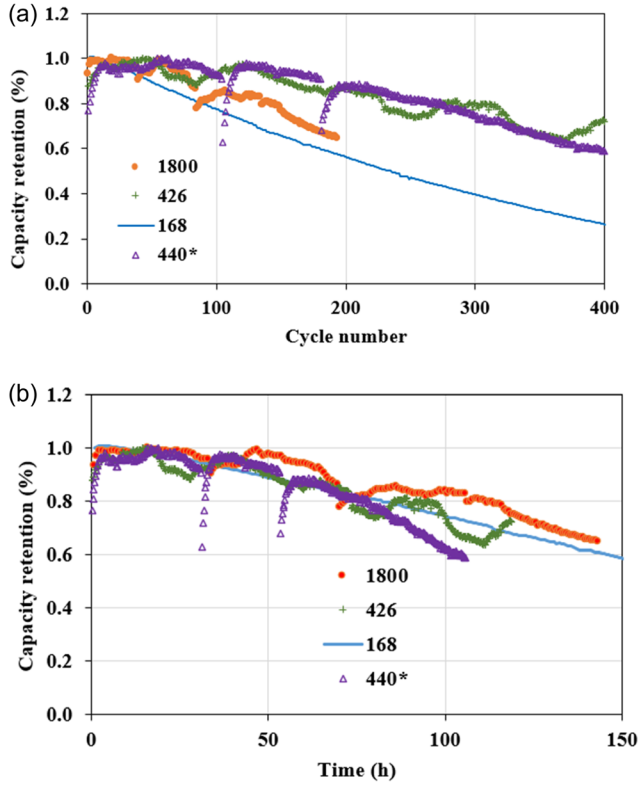

Figure 7. Comparison of results from cells of four different sizes, namely, 1800 cm^2 (Case #12) using graphite sheets, 426 cm^2 (Case # 8) using graphite plates, 168 cm^2 (Case #13) using graphite sheets and 440 cm^2 (Case #9) using graphite sheets, all at a current density of 125 mA cm^{-2} except for case #9 which was at 150 mA cm^{-2}: normalized discharge capacity variation as a function of a) cycle number and b) time. In each case, the discharge capacity has been normalized by dividing by the maximum value during the test. The sudden dips in the discharge energy in Case #9 at 31.3 and 53.5 h were caused by brief stoppage of the testing to change headers in the peristaltic pumps.

capacity of all cycles in the test. Figure 7a shows the variation of the normalized discharge capacity with the cycle number for the four cells while Figure 7b shows the variation as a function of time. The sudden dips in discharge capacity in the data of Case #9 at cycle number 105 (cycle time of 31.3 h) and cycle number 181 (cycle time of 53.5 h) were due to brief stoppages of cycling to allow change of header tubing of the peristaltic pumps. It is interesting to note that it takes several (≈10) cycles for the discharge energy to come back to recover completely. It is also interesting to note that the data of Cases #8 and #9, both from cells of about the same size, follow the same trend, qualitatively and quantitatively, in both Figure 7a,b, i.e., in terms of both cycle number and cycling time. Both these cases however show substantial deviation from the capacity fade data of 168 and 1800 cm^2 cell data in Figure 7a. One reason for this the probably the cycle time. When the capacity data are plotted in terms of test duration in Figure 7b, one can see fairly good and overlapping trend of capacity fade. Thus, on a temporal basis, there is no significant effect of cell size on the capacity fade. On a per-cycle basis, all the four cells have shown a capacity retention of 60% or higher at the end 200 cycles, which is higher than those reported in the literature (see Table 2) where typically small cell size data only have been reported. On the face of it, for a given cell potential, the current density should not depend on the cell size, all other parameters being equal. This "point model" is applicable to cells of small size. However, large cells deviate from this point model and may show significant spatial variation of current density due to the local variation of the SoC. In addition, large cells are not operated at the same area-specific electrolyte circulation rate as small cells because of the significantly higher pressure drop encountered in large cells. The effective SoC range in which the cell is operated may be narrower in large cells. All these factors can contribute to capacity fade differences in small and large cells and may explain the differences between our data and those reported in the literature for cells of 100 cm^2 or less.

Capacity fade data from the 13 runs spanning three current densities, four cell sizes, different electrolyte circulation rates and different electrolyte volume to cell size ratio are compared in Table 2. The last two columns show two metrics of capacity fade measure. The first one, namely, per cent capacity fade per cycle, was evaluated as

$$F_1 = \text{per cent capacity fade per cycle} = \frac{(\text{First cycle capacity} - \text{last cycle capacity}) \times 100}{(\text{First cycle capacity} \times \text{no. of cycles})} \quad (6)$$

The second metric, capacity fade flux, was evaluated as

$$F_2 = \text{capacity fade flux} = \frac{(\text{First cycle capacity} - \text{last cycle capacity})}{(\text{area of cell} \times \text{total duration of test})} \quad (7)$$

Numerical values of these metrics are listed in the last two columns of Table 2 for each case. The average value and the standard deviation are also listed at the bottom of each column. While both vary significantly from case to case, the standard deviations shows that the variation is not too much. Thus, one can conclude that in industrial-scale VRFB cells operating in the current density range of 75–125 mA cm^{-2} at reasonably low and achievable circulation rates (for example where the pumping power is of the order 5% to 10% or less of the operating power of the cell[27]), the capacity fade per cycle is about 0.15% and the capacity fade flux is about 1 Ah (m^{-2} h).

2.4. Variation of Concentration of Vanadium Ions

Measurement of the concentration of vanadium ions, together with weight change in the positive and negative electrolyte tanks, shows that long-duration cycling led to a net transport of vanadium species from the negative electrolyte to the positive electrolyte in the present case, where the cells had a cation-conducting membrane (Nafion 117). This observation was also supported by the steady increase in the open circuit voltage as the testing progressed. The increase in the OCV was consistent with the value predicted from the Nernst Equation (see Equation (10)) using measured concentrations of vanadium ions on each side. As may be expected, no V(III) was found on the positive side at any stage after the initial charging of the equi–molar mixture of V(III) and V(IV) electrolyte. Similarly, no V(IV) was found on the negative side after initial charging. Mole balance estimations showed that there was a net movement of vanadium ions from the negative side to the positive side.

The variation of the concentration of vanadium ions is highly dependent on initial conditions and conditions of operation (such as operating current density). However, after 100 or more cycles, the cell usually reached an asymptotic pattern of capacity fade in which the concentration, at the end of successive discharge steps, of V(V) kept increasing and that of V(IV) kept decreasing steadily on the positive side while the concentration of V(III) on the negative side kept decreasing, although at a lower rate than V(IV). One may attribute this to the difference in vanadium ion diffusivities in the following way. Measurements reported in the literature[9] show that the diffusivity of the ions through the Nafion membrane is typically in the following order: V(II) > V(IV) > V(V) > V(III). The higher diffusive flux of V(II) leads to generation of V(IV) through the self-diffusion reaction (Equation ((4a)) above) on the positive side; however, in the following charging step, most of these ions get converted to V(V), while some (more than V(V)) diffuse to the negative side leading to a depletion of V(IV) on the positive side. At the same time, due to depletion of V(II) on the negative side (due to their higher rate of cross-over), V(V) cannot be fully converted to V(IV) in the subsequent discharge step, and they therefore accumulate on the positive side. The lower diffusivity of V(III) ions compared to the other vanadium ions of interest means that their loss by cross-over is less and the loss in production during discharge is somewhat compensated by the diffusion of vanadium ions from the positive side (as per reactions (5a) and (5b) above). While this scenario is plausible, more experimental and modeling studies are needed to

confirm it. Many additional factors have been adduced in the literature for capacity fade,[10,19] including ion migration, convection, osmosis, and reverse osmosis. Detailed modeling of these phenomena will be needed to understand and predict capacity fade in industrial-scale systems. It is expected that the present data will prove useful in validating and calibrating such mathematical models.

3. Conclusion

Long-duration capacity fade studies have been conducted in medium- and large-sized vanadium redox flow battery cells in the constant current density range of 75–125 mA cm^{-2}, voltage limits of [0.9, 1.7 V] and at circulation rates suited for good hydrodynamic and electrochemical performance. The following conclusions can be drawn from these studies: 1) Although there is some variation with current density and circulation rate, the average capacity fade per cycle is (0.15 ± 0.06)%. This value is much lower than what has been reported based on laboratory-scale cells. 2) The average capacity fade flux over the dozen cases covering cell areas in the range of 168–1800 cm^2 is (1.0 ± 0.5) Ah (m^{-2} h). This flux is higher for smaller cell sizes. 3) Long-duration cycling led to a net transport of vanadium species from the negative electrolyte to the positive electrolyte in the present case where the cells had a cation-conducting membrane (Nafion 117). This observation was also supported by sustained increase in the open circuit voltage which was consistent with variation of vanadium ion concentration. 4) While the concentration of vanadium ions is highly dependent on initial conditions and conditions of operation, the cell reaches an asymptotic pattern of capacity fade in which the concentration V(V) keeps increasing and V(IV) decreasing on the positive side while the concentration of V(III) on the negative side keeps decreasing, although at a lower rate than V(IV), at the end of successive discharge steps.

The results of the present study are in broad agreement with observations reported earlier in the literature. A net, sustained increase of about 30% over 300 cycles in the total vanadium content in the positive electrolyte and a corresponding decrease in the negative electrolyte for one experimental run was reported earlier by Sun et al.[10] in a 15-cell stack. Their report of net water migration of about 25% toward the positive electrolyte tank is also consistent with the present results. The experimental results of Bo et al.[10] in a small cell of up to 50% volume change toward the positive side and about 50% capacity fade over 200 cycles agree with the present results. In neither case, the variation of the concentration of individual vanadium ion was reported. The recent modeling study of Xiong et al.[28] predicts a mixed set of results. The volume of electrolyte in the positive tank was predicted to increase by about 5% only over the first 50–100 cycles and remain constant thereafter. (A similar saturation of the electrolyte volumes, but with larger difference in volumes, was observed in Case #10 of the present data set.) Their result for a single showed that the concentration of of V(III) increased marginally, that of V(V) decreased marginally over 200 cycles while those of V(IV) and V(II) reduced more substantially over the same period. The capacity fade model of Zou et al.[19] also showed contradictory results. While their prediction of increase in electrolyte volume is consistent with the present results, the predicted increase in capacity fade with increase in current density is contrary to the present experimental results as well as those of Huang et al.[18]

The following generic observation can be made in the light of the present results. For a given cell of given architecture (and thus, the area specific resistance), the concentrations of vanadium ions of different oxidation states depend on a number of factors including the volume of electrolyte, the electrolyte circulation rate, the current density employed, the voltage limits enforced, etc. Acid concentration and cell temperature too will have a role to play. This will have a subsequent effect on the quantity of diffusion and migration fluxes leading to different evolutions of the capacity over time for different cases. Such effects can be understood quantitatively only through a detailed phenomenological modeling accounting for all the underlying causes and effects. It is hoped that the present experimental results for more than a dozen cases will be useful in developing improved, multieffect phenomenological models for capacity fade.

4. Experimental Section

Construction of Cells

The construction of the VRFB cells follows the procedure described in our previous studies[21,22,25] and is briefly outlined here. The medium size (426 cm^2 active area) single-cell VRFB was fabricated using SIGRACELL GFD 4.65 EA activated carbon felt (of 6 mm thickness compressed to 3 mm) as electrode on both sides, SGL graphite plate (SGL R7650) with serpentine flow field serving as bipolar plates, Nafion−117 membrane serving as both separator of the electrolytes and proton conductor, and copper plate current collectors. The graphite plates had a single serpentine flow field of 4 mm width, 3 mm depth, and 3 mm rib width grooved using a computer-controlled milling machine. Silicone gasket of 3 mm thickness was used in several layers to prevent leakage and mixing. Further, the ion-exchange membrane was made to protrude about 2 cm on all four sides of the rectangular cell to prevent direct mixing of the electrolytes. To prevent leakage, aluminum end plates were tightened using multiple nut and bolt pairs.

The 1800 cm^2 area cell was constructed using the same materials except for the bipolar plate which was made of thin expanded graphite sheet (SGL Carbon TF6) of 0.6 mm thickness. Since flow channels cannot be grooved on to such a thin bipolar plate, the cell is of flow-through mode design[25] in which all the electrolyte is forced to flow through the porous electrode on each side. An 8 mm-thick polypropylene flow frame with a 1 mm-thick silicone gasket on either side was used to create a 10 mm-thick electrode made of three layers of 4.6 mm-thick SIGRACELL carbon felt. In order to ensure uniform compression over the entire electrode area, several 2 cm-wide strips of the expanded graphite sheet were placed over the electrode area. A header area of width of 15 mm was provided at entry and exit from the electrode region and the inlet/ outlet piping was connected to these headers through the sides of the flow frame.

In all cases of cell assembly, no special measures have been taken to activate either the membrane or the electrode via the catalytic[22] or thermal[23] routes. For a given cell, the same membrane and electrode

felts have been used repeatedly. After each disassembly of a cell, the membrane and the electrodes were washed thoroughly with deionized (DI) water; the membrane was kept fully immersed in DI water during storage. The electrodes were allowed to dry in ambient air and were thoroughly wetted during the subsequent assembly. In all cases, fresh electrolyte was circulated for at least one hour before starting the charging of the cell so as to ensure good wettability of the electrolytes and hydration of the membrane.

Experimental Protocol

At the beginning of the experiment, the electrolyte on both sides consisted of an equimolar (0.8 M each) mixture of V(IV) and V(III) in 4.2 M H_2SO_4. The electrolyte in as-procured condition (from Oxkem Ltd, UK) was used without further modification (such as dilution or additives). After flushing the cell with DI water and then with the same pristine electrolyte solution on each side, a fresh quantity of the electrolyte was taken for charge–discharge cycling. For the medium-sized cell, 426 ml of the Oxkem electrolyte was used on each side; for the 1800 cm^2 cell, due to its thicker electrode, 3.1 L of Oxkem electrolyte was used on each side. In the medium-size cell, a circulation rate of 330 ml min^{-1} was used in all experiments, unless mentioned otherwise. In the large cell case, the flow rate was maintained at 1250 ml min^{-1} which corresponded to electrolyte superficial circulation velocity of 5 mm s^{-1} (which can be considered as sufficiently high to maintain good electrochemical performance[25]). Peristaltic pumps were used for circulation of the electrolytes; a few experiments were conducted using diaphragm pumps in the medium-size cell case.

The capacity fade experiments started with initial charging of the electrolytes at 60 mA cm^{-2} up to cell voltage of 1.75 V followed by further charging to the same voltage limit at a current density of 30 mA cm^{-2}. Typically, the total charge transferred to the electrolyte was in excess of 95% of the theoretical capacity (after accounting for the charge required to convert V(III) to V(IV) on the positive side and V(IV) to V(III) on the negative side. The cell was then deep discharged to 0.8 V at a current density of 60 mA cm^{-2}. With this as the initial condition, the cell was then subjected to constant-current successive charge–discharge cycling in the operating voltage range of [0.9, 1.7 V] with a 75 s rest period between each step to measure the open circuit voltage of the cell. Nitrogen was continuously bubbled through the negative side electrolyte tanks throughout the experiment in order to avoid oxidation of the electrolyte in the presence of air.

Data Acquisition and Curation

Each capacity fade experiment ran for several days. The following data were measured periodically over this period: 1) A Bitrode battery cycler was used for cell voltage control. The cell voltage and the applied current were measured every second and averaged values over a 10-second interval were stored for further data processing. The data cycler would complete the charging/ discharge step as soon as the set voltage limit was reached. It would then go into a time-limited rest period after which it would go the subsequent discharge/ charge step if the cycle count had not exceeded the preset limit, typically set to 400. 2) Both electrolyte tanks were mounted on individual electronic weighing balances. These were set to zero at the beginning of the experiment. Subsequently, the displayed weight was recorded manually at intervals of 20–25 cycles. 3) After a set number of charge–discharge cycles (typically 20), 250 µL samples of each electrolyte were collected during the rest period at the end of the charging and discharging steps. These were analyzed later using Ultraviolet-visible (UV-vis) spectroscopy[26] to determine the concentrations of V(V), V(IV), V(III) and V(II) species. Of the four vanadium ion species, V(II) is susceptible to oxidation during the manual transfer of the sample to the testing vial during the UV–vis measurements. This would have led to erratic results. Keeping this mind, we report here the data of negative side ion concentrations only at the end of discharge step at which time most of V(II) would have been converted to V(III) by the electrochemical reaction. In most cases, the measured concentration of V(II) was indeed close to zero.

Using the data of time, cell voltage, current, step number, and cycle number collected from the battery cycler, the charging and discharging capacity and energy change were evaluated for each cycle. The total capacity and energy exchange reported by the battery cycler were used to calculate the coulombic efficiency and the round-trip energy efficiency from which the voltaic efficiency was estimated.[23,25] From measured vanadium ion concentrations, the SOC was estimated at the end of the charge and discharge steps was evaluated as

$$SOC_c = \frac{C_{VO_2^+{}_c}}{C_{VO_2^+{}_c} + C_{VO^{2+}{}_c}} \tag{8}$$

$$SOC_d = \frac{C_{VO_2^+{}_d}}{C_{VO_2^+{}_d} + C_{VO^{2+}{}_d}} \tag{9}$$

here, $C_{VO_2^+{}_c}$ and $C_{VO^{2+}{}_c}$ are the concentrations of V(V) and V(IV) at the end of charging and discharging steps on the positive side, respectively. Similarly, $C_{VO_2^+{}_d}$ and $C_{VO_2^+{}_d}$ the are the corresponding concentrations at the end of the discharge step.

The OCV was measured using battery cycler during the rest period after each charge and discharge step and is reported here at an interval of 20–25 cycles as the change over a single cycle was less than the detectable limit of the battery cycler. Additionally, the OCV of the battery was theoretically estimated using the Nernst equation and the measured concentration of the vanadium species

$$OCV = E^0 + \frac{RT}{nF}\ln\left(\frac{C_{VO_2^+} \cdot C_{V^{2+}} \cdot C_{H^+}^2}{C_{VO^{2+}} \cdot C_{V^{3+}}}\right) \tag{10}$$

where E^0 is the standard electrochemical potential in Volts (V), R is the universal gas constant having a value of 8.314 J $(mol\ K)^{-1}$, T is the temperature in Kelvin (K), n is the charge number, F is Faraday's constant having a value of 96,486 A (mol s), $C_{V^{3+}}$ is the concentration of V^{3+}, $C_{V^{2+}}$ is the concentration of V^{2+}, and C_{H^+} is the concentration of H^+. In evaluating the OCV, the measured species concentrations were used while the concentration of H^+ was estimated based on the sulfuric acid concentration, assuming complete dissociation into sulfate ions.

Acknowledgements

The work described in this article was funded by grants from MHRD (grant reference no. F.NO.41-2/2015-T.S.-I (Pt.)) and DST-Solar Energy Harnessing Centre (grant reference no. DST/TMD/SERI/HUB/1(C)), both of Government of India.

Conflict of Interest

The authors declare no conflict of interest.

Data Availability Statement

The data that support the findings of this study are available from the corresponding author upon reasonable request.

Keywords: capacity fade · ion transfer · open circuit voltage · ultraviolet-visible spectroscopy · vanadium ions concentration · vanadium redox flow battery

[1] T. M. Gur, *Energy Environ. Sci.* **2018**, *11*, 2696.
[2] J. Liu, X. Chen, S. Cao, H. Yang, *Energy Convers. Manag.* **2019**, *187*, 103.
[3] P. Alotto, M. Guarnieri, F. Moro, *Renew. Sustain. Energy Rev.* **2014**, *29*, 325.
[4] K. Mongird, V. Viswanathan, J. Alam, C. Vartanian, V. Sprenkle, R. Baxter, Grid Energy Storage Technology Cost and Performance Assessment. Technical Report No. DOE/PA-0204, US Department of Energy, Washington, DC **2020**.
[5] P. K. Vudisi, S. Jayanti, R. Chetty, *Batteries* **2022**, *8*, 85.
[6] T. Mohammadi, S. C. Chieng, M. S. Kazacos, *J. Membr. Sci.* **1997**, *133*, 151.
[7] T. Sukkar, M. Skyllas-Kazacos, *J. Membr. Sci.* **2003**, *222*, 249.
[8] E. Wiedemann, A. Heintz, R. N. Lichtenthaler, *J. Membr. Sci.* **1998**, *141*, 207.
[9] C. Sun, J. Chen, H. Zhang, X. Han, Q. Luo, *J. Power Sources* **2010**, *195*, 890.
[10] S. N. Oreiro, A. Bentien, J. Sloth, M. Rahimi, M. B. Madsen, T. Drechsler, *Chem. Eng. J.* **2024**, *490*, 151947.
[11] W. Dai, Y. Shen, Z. Li, L. Yu, J. Xi, X. Qiu, *J. Mater. Chem. A* **2014**, *2*, 12423.
[12] Z. Li, W. Dai, L. Yu, L. Liu, J. Xi, X. Qiu, L. Chen, *ACS Appl. Mater. Interfaces* **2014**, *6*, 18885.
[13] J. Bo, L. Wu, L. Yu, X. Qiu, J. Xi, *J. Membr. Sci.* **2016**, *510*, 18.
[14] O. Nibel, T. J. Schmidt, L. Gubler, *J. Electrochem. Soc.* **2016**, *163*, A25703j.
[15] A. Bhattarai, P. C. Ghimire, A. Whitehead, R. Schweiss, G. G. Scherer, N. Wai, H. H. Hng, *Batteries* **2018**, *4*, 1.
[16] S. Maghsoudy, M. Rahimi, A. M. Dehkordi, *J. Energy Storage* **2022**, *54*, 105347.
[17] X. Chen, J. Xi, K. Ma, L. Liu, *J. Power Sources* **2023**, *556*, 232442.
[18] Z. Huang, Y. Liu, X. Xie, C. Huang, Q. Huang, Z. Guo, Y. Liu, *J. Electrochem. Soc.* **2024**, *171*, 010521.
[19] W.-J. Zou, Y.-B. Kim, S. Jung, *Appl. Energy* **2024**, *356*, 122329.
[20] T. Ma, Z. Huang, B. Li, X. Xie, C. Huang, T. Lin, Z. Guo, *J. Electrochem. Soc.* **2024**, *171*, 060503.
[21] R. Gundlapalli, S. Jayanti, *J. Power Sources* **2019**, *427*, 231.
[22] P. K. Vudisi, S. Jayanti, R. Chetty, *Fut. Batt.* **2025**, *5*, 100052.
[23] P. K. Vudisi, S. Jayanti, R. Chetty, *J. Energy Storage* **2023**, *72*, 108734.
[24] R. Monteiro, J. Leirós, M. Boaventura, A. Mendes, *Electrochim. Acta* **2018**, *267*, 80.
[25] M. M. Prasanna, S. Jayanti, *J. Power Sources* **2023**, *582*, 233536.
[26] S. S. Kumar, S. Jayanti, *Direct Measurement of Energy Storage Capacity of Vanadium Redox Flow Battery Using UV-Vis Spectroscopy, in: ASTFE Digital Library*, Begell House Inc., Danbury, CT **2024**, https://dl.astfe.org/conferences/tfec2024,2d6c7309626b1193,47f0cef02723657c.html.
[27] M. M. Prasanna, S. Jayanti, *J. Power Sources* **2025**, *631*, 236203.
[28] R. Xiong, B. Xiong, Q. Zhang, S. Shi, Y. Su, D. Zhang, *Int. J. Green Energy* **2022**, *19*, 1613.

Manuscript received: June 11, 2025
Revised manuscript received: August 29, 2025
Version of record online: